Pharmacological Research 188 (2023) 106639

Contents lists available at ScienceDirect

Pharmacological Research

journal homepage: www.elsevier.com/locate/yphrs

# Augmented efficacy of nano-formulated docetaxel plus curcumin in orthotopic models of neuroblastoma

Martina Di Francesco [a,1], Fabio Pastorino [b,1], Miguel Ferreira [a,1], Agnese Fragassi [a,c], Valentina Di Francesco [a,d], Anna Lisa Palange [a], Christian Celia [e,f], Luisa Di Marzio [e], Michele Cilli [g], Veronica Bensa [b], Mirco Ponzoni [b,2], Paolo Decuzzi [a,*,2]

[a] Laboratory of Nanotechnology for Precision Medicine, Fondazione Istituto Italiano di Tecnologia, Genova, Italy
[b] Laboratory of Experimental Therapies in Oncology, IRCCS Istituto Giannina Gaslini, Genova, Italy
[c] Department of Chemistry and Industrial Chemistry, University of Genova, Genoa, Italy
[d] Department of Informatics, Bioengineering, Robotics and System Engineering, University of Genoa, Via Opera Pia, 13, 16145 Genoa, Italy
[e] Department of Pharmacy, University of Chieti – Pescara "G. d'Annunzio", 66100 Chieti, Italy
[f] Lithuanian University of Health Sciences, Laboratory of Drug Targets Histopathology, Institute of Cardiology, A. Mickeviciaus g. 9, LT-44307 Kaunas, Lithuania
[g] Animal Facility, IRCCS Ospedale Policlinico San Martino, Genoa, Italy

ARTICLE INFO

*Keywords:*
Neuroblastoma
Nanoparticles
Curcumin/Docetaxel
Combination therapy
Drug delivery

ABSTRACT

Neuroblastoma is a biologically heterogeneous extracranial tumor, derived from the sympathetic nervous system, that affects most often the pediatric population. Therapeutic strategies relying on aggressive chemotherapy, surgery, radiotherapy, and immunotherapy have a negative outcome in advanced or recurrent disease. Here, spherical polymeric nanomedicines (SPN) are engineered to co-deliver a potent combination therapy, including the cytotoxic docetaxel (DTXL) and the natural wide-spectrum anti-inflammatory curcumin (CURC). Using an oil-in-water emulsion/solvent evaporation technique, four SPN configurations were engineered depending on the therapeutic payload and characterized for their physico-chemical and pharmacological properties. All SPN configurations presented a hydrodynamic diameter of ~ 185 nm with a narrow size distribution. A biphasic release profile was observed for all the configurations, with almost 90 % of the total drug mass released within the first 24 h. SPN cytotoxic potential was assessed on a panel of human neuroblastoma cells, returning $IC_{50}$ values in the order of 1 nM at 72 h and documenting a strong synergism between CURC and DTXL. Therapeutic efficacy was tested in a clinically relevant orthotopic model of neuroblastoma, following the injection of SH-SY5Y-Luc$^{+}$ cells in the left adrenal gland of athymic mice. Although ~ 2 % of the injected SPN per mass tissue reached the tumor, the overall survival of mice treated with CURC/DTXL–SPN was extended by 50 % and 25 % as compared to the untreated control and the monotherapies, respectively. In conclusion, these results demonstrate that the therapeutic potential of the DTXL/CURC combination can be fully exploited only by reformulating these two compounds into systemically injectable nanoparticles.

## 1. Introduction

Neuroblastoma (NB) represents the most frequent and aggressive form of extracranial solid tumor in infants and is responsible for 15% of all the childhood cancer deaths [1,2]. Chemoradiotherapy remains the primary treatment choice, often exposing patients to unacceptable toxicity and the progressive build-up of drug resistance [2,3]. The non-specific intratissue accumulation of conventional chemotherapeutic drugs is the main cause of short-term and long-term toxicity, which inevitably limits the administered drug dose and the efficacy of the intervention [4,5]. As a consequence, the 5-year survival rate for high-risk NB patients is below 50 % [2,6], and the identification of more potent and less toxic therapies is urgently needed [2]. New therapeutic strategies should simultaneously target malignant cells and the tumor microenvironment, which includes multiple immune and stromal cells – macrophages, dendritic cells, mast cells, natural killer cells, T and B

* Corresponding author.
*E-mail address:* paolo.decuzzi@iit.it (P. Decuzzi).
[1] MDF, FP, and MF contributed equally to this work.
[2] MP and PD share the senior authorship.

https://doi.org/10.1016/j.phrs.2022.106639
Received 15 August 2022; Received in revised form 21 December 2022; Accepted 27 December 2022
Available online 28 December 2022
1043-6618/© 2022 The Authors. Published by Elsevier Ltd. This is an open access article under the CC BY-NC-ND license (http://creativecommons.org/licenses/by-nc-nd/4.0/).

cells, cancer-associated fibroblasts (CAFs), mesenchymal stromal cells (MSCs) and Schwann cells [7]. The cross-talk among these cells promotes inflammation, angiogenesis, and the alteration of the extracellular matrix sustaining tumor progression and metastasis formation [7–9]. Combination therapies represent an interesting approach for NB as they allow the simultaneous targeting of different cell types within the malignant mass.

Promising anti-cancer combination therapies rely on the association of cytotoxic drugs with anti-inflammatory molecules, which could boost the potency of the chemotherapeutic drug by modulating the drug resistance of cancer cells and also act on the tumor microenvironment [10,11]. Indeed, in previous studies, the authors and others have shown that the co-administration of the COX-2 inhibitor celecoxib or the natural compound curcumin (CURC) with chemotherapeutic drugs, such as doxorubicin, etoposide, irinotecan, cisplatin, docetaxel, vincristine, increases the efficacy of the intervention [11–14]. Most neuroblastoma cells tend to overexpress COX-2 and NF-kβ, which correlates with *in vitro* enhanced cell proliferation and migration, and *in vivo* increased growth rate of the malignant mass [15–17]. Specifically, Zhi et al. demonstrated that NF-kβ is over-expressed in the human neuroblastoma cell line SH-SY5Y and promotes tumor cell migration and invasion through the up-regulation of the CXC chemokine receptor-4 (CXCR4) [18]. In general, the effect of CURC on the NB cells is modest, returning $IC_{50}$ values in the several μM range, but it acts on multiple pathways, including NF-kβ, WNT/β-catenin, PI3K/Akt, Caspases, p53 and p21 [19–22]. In particular, by inhibiting the AKT pathway and downregulating COX-2 and NF-kβ, which are overexpressed in several cancers including neuroblastoma [12,15,18,23,24], CURC can affect the sensitivity of the cancer cells to chemotherapy (drug resistance) as well as modulate the expression of the matrix metalloproteinase-9 and adhesion receptors (tumor microenvironment), which have been involved with cancer cell invasion and metastasis [19–22]. Thus, all these observations would encourage testing the combination of CURC with a potent chemotherapeutic drug in the treatment of neuroblastoma [13,25].

Among several candidates, docetaxel (DTXL) is an interesting molecule as it is already used in the treatment of pediatric solid tumors – osteosarcoma, soft tissue sarcoma, and others [13,26–29]. DTXL interferes with cell mitosis by suppressing the microtubule dynamics and arresting the cell cycle in the G2/M phase [28]. However, despite its efficacy, the application of DTXL is limited by its severe systemic toxicity, including neutropenia, diarrhea, nausea, and fatigue [27,30]. Notably, DTXL induces NF-kβ activation and COX-2 overexpression, which are both involved in cell survival and drug resistance [25,31,32]. In this context, the combination of DTXL with the broad-spectrum anti-inflammatory molecule CURC appears to be a promising strategy. Here, nanoparticles are designed to deliver the combination of DTXL and CURC directly to the malignant mass, limiting non-specific accumulation within the bone marrow and other sensitive organs while preserving the optimal mass ratio between the two molecules [33,34]. Specifically, biodegradable PLGA spherical nanomedicines (SPN) were engineered, characterized *in vitro*, and validated *in vivo* for the CURC/DTXL combination therapy of orthotopically implanted neuroblastoma masses. It was demonstrated that the drug combination returns a higher therapeutic efficacy, as compared to the DTXL monotherapy, and reduced side effects.

## 2. Materials and methods

### 2.1. Materials

Poly(D,L-lactide-co-glycolic) acid (PLGA, 50:50, Carboxy Terminated, MW ~ 60 kDa), 1,2-dipalmitoyl-sn-glycero-3-phosphocholine (DPPC) and 1,2-distearoyl-sn-glycero-3-phosphoethanolamine- N-[succinyl(polyethylene glycol)-2000] (DSPE-PEG), dimethyl sulfoxide (DMSO), 3-(4,5-Dimethyl-2-thiazolyl)-2,5-diphenyl-2H-tetrazolium bromide (MTT), human fibronectin, acetonitrile (ACN), chloroform and other solvents were purchased by Sigma-Aldrich (Saint Louis, Missouri, USA). Docetaxel (DTXL) and Curcumin (CURC) were obtained from Alfa Aesar (Haverhill, Massachusetts, USA). High-glucose Dulbecco's modified Eagle's minimal essential medium (DMEM), RPMI- 1640, penicillin-streptomycin solution, glutamine and heat inactivated fetal bovine serum (FBS) were purchased from Gibco (Invitrogen Corporation, Giuliano Milanese, Milan, Italy). DOTA-NHS was purchased from CheMatech (France), and Copper ($^{64}$Cu) Chloride (15 mCi, in 1 mL) was purchased from ACOM (Montecosaro, Italy).

### 2.2. Synthesis of Spherical Polymeric Nanomedicines (SPN)

Empty and drug-loaded SPN were synthesized using an oil-in water emulsion/solvent evaporation technique as previously reported by the authors [35]. Briefly, an organic phase containing 170 μL of poly (lactic-co-glycolic acid) (PLGA) (60 mg/mL in chloroform) and 90 μL 1,2-dipalmitoyl-sn-glycero-3-phosphocholine (DPPC) (10 mg/mL in chloroform) was added drop by drop into 10 mL of aqueous phase containing 110 μL of 1,2-distearoyl-sn-glycero-3-phosphoethanolamine-N-[carboxy(polyethylene glycol)-2000] (DSPE-PEG) (10 mg/mL in 4 % v/v EtOH) and sonicated for 1 min and 30 s at 100% amplitude using probe sonicator (Q125 sonicator, Q-Sonica). In the case of DTXL–SPN, CURC–SPN and CURC/DTXL–SPN, 200 μL of DTXL solution (10 mg/mL in chloroform), 400 μL of CURC solution (2.5 mg/mL in chloroform) and 150 μL of DTXL solution plus 250 μL of CURC solution were added to the organic phase, respectively. The emulsion was placed under magnetic stirring, and after complete solvent evaporation, the resulting particles were purified through different centrifugation steps. First, to remove debris resulting from the synthesis process, SPN were centrifuged at low speed (452 × *g* for 5 min) then, to remove the unloaded drug, the resultant supernatant was centrifuged at high speed for two times (18,213 × *g* for 15 min). In order to label SPN with the near-infrared dye Cy5, 20 % of the DSPE-PEG amount used for nanoparticle synthesis was replaced by DSPE-CY5 (0.02 mg, Lip-Cy5), realized following previous works by the authors [36]. The SPN pellet was stored at 4 °C.

### 2.3. Labeling SPN with $^{64}$Cu

Biodistribution experiments were realized injecting intravenously SPN labeled with $^{64}$Cu. For the preparation of $^{64}$Cu-SPN, 20 % of DSPE–PEG amount used for the SPN synthesis was replaced by DSPE–DOTA. The resulting DOTA–SPN were left to react with 500 μCi of $^{64}$Cu solution for 2 h in acetate buffer at 37 °C. The non-reacted $^{64}$Cu was removed from the solution *via* four sequential centrifugation steps (washed initially in PBS (2 ×) followed by DI water (2 ×), centrifugation for 15 min at 12,400 rpm).

### 2.4. SPN physico-chemical characterization

The size, size distribution, and surface zeta potential (ζ) of SPN were measured *via* a dynamic light scattering (DLS) Zetasizer Nano system (Malvern, UK). Samples were diluted with isotonic double distilled water (1:10 v/v) to avoid multiscattering and analyzed at 25 °C. Particle stability was evaluated in PBS buffer at 37 °C for up to 4 days. At each time point, samples were analyzed at DLS as reported above. Also, the size and shape of SPN were analyzed using a Scanning Electron Microscope (SEM). Briefly, a drop of nanoparticle solution was deposited on a silicon wafer, dried, sputtered using gold, and mounted on a stab for SEM analysis. SEM images were collected *via* a JEOL JSM-7500FA (Jeol, Tokyo, JAPAN), operating at 5–15 kV of accelerating voltage.

### 2.5. SPN drug loading

High Performance Liquid Chromatography (HPLC) (Agilent 1260 Infinity, Germany) was used to evaluate drug loading into SPN. For all

the SPN configurations (CURC-DTXL, DTXL-SPN, CURC/DTXL-SPN), the same standard protocol was used [35]. Briefly, drug-loaded SPN were dissolved in a mixture of acetonitrile (AcN)/$H_2O$ (1:1, v/v) to promote the release of the entrapped drug. The HPLC was equipped with a 100 μL sample loop injector and with a C18 column (4.6 × 250 mm, 5 μm particle size, Agilent, USA) for chromatographic separation. An isocratic condition ($H_2O$ + 0.1 % (v/v) TFA/AcN + 0.1 % (v/v) TFA, 43:57 v/v, 0.3 mL/min) was applied for the elution of both drugs. CURC and DTXL were analyzed at λ = 430 and 230 nm, respectively. The drug loading defined as the ratio between the amount of drug loaded in the nanoparticles (*i.e.*: dispersed in the PLGA polymeric matrix after the purification steps) and the total mass of the SPN.

### 2.6. SPN drug release

The release profiles of CURC and DTXL from SPN, either alone or combined into CURC/DTXL-SPN, were studied upon particle exposure to a 4-L PBS solution, mimicking an infinite sink condition. Briefly, 200 μL CURC–SPN, DTXL–SPN, or CURC/DTXL–SPN were placed into Slide-A-Lyzer MINI dialysis microtubes with a molecular cutoff of 10 kDa (Thermo Scientific, USA) and then dialyzed against 4 L of PBS buffer (1 ×, pH = 7.4, 37 ± 2 °C). At specific time points, three samples were collected and centrifuged (18,213 × *g* for 20 min). Then, pellets were dissolved and analyzed in HPLC as reported above for the SPN drug loading.

### 2.7. Cell culture

The human neuroblastoma (NB) cell lines SH-SY5Y, IMR-32, HTLA-230, and LAN-5 were grown in high-glucose Dulbecco's modified Eagle's minimal essential medium (DMEM) or RPMI-1640, with 10 % (v/v) heat-inactivated FBS, 1 % glutamine, and 1 % (v/v) penicillin/streptomycin solution, as previously described [37,38]. Cells were infected with retrovirus expressing the firefly luciferase (Luc) gene, as previously reported [39]. Luciferase activity of the Luc-transfected cells was confirmed by bio-luminescent imaging (BLI, Lumina-II, Caliper Life Sciences, Hopkinton, MA) after a 10 min incubation with 150 μg/mL D-luciferin (Caliper Life Sciences) diluted in cell culture medium, as previously described [37–39]. Cells were tested for mycoplasma contamination, characterized by cell proliferation and morphology evaluation, and authenticated at time of experimentation by multiplex STR-profiling test (PowerPlex® Fusion, Promega, Milan, Italy) by BMR Genomics (Padova, Italy) and validated using ATCC STR, DSMZ STR and NCBI databases.

### 2.8. SPN cytotoxicity on human neuroblastoma cells

To assess the cytotoxic effect of CURC and DTXL, either alone or combined and either in the form of free molecules or encapsulated in SPN, Luc-transfected SH-SY5Y, IMR-32, LAN-5 and HTLA-230 cells were seeded overnight in a 96-well culture plates at a density of 10,000 cells/well. The NB cells were then exposed to different concentrations of free CURC, free DTXL, free CURC/DTXL, empty SPN, CURC-SPN, DTXL-SPN, and CURC/DTXL-SPN or empty SPN matching the different CURC/DTXL-SPN concentrations. At 24, 48, and 72 h, the culture medium was removed and a MTT solution (5 mg/mL in PBS buffer) was added to each well according to the instructions of the manufacturer. The absorbance of formazan crystals dissolved in EtOH was quantified using a microplate spectrophotometer at a wavelength of 570 nm, using 650 nm as the reference wavelength (Tecan, Mannedorf, Swiss). The percentage of cell viability was assessed according to the following equation:

$$CellViability(\%) = \frac{Abs_t}{Abs_c} \times 100 \quad (1)$$

where $Abs_t$ is the absorbance of the treated cells and $Abs_c$ is the absorbance of the control (untreated) cells. $IC_{50}$ was calculated by Graphpad Prism software v.5 (GraphPad Software, USA).

For assessing possible additive/synergistic interactions between CURC and DTXL, either as free molecules or encapsulated into SPN, isobolograms were generated [35]. The Combination Index (CI), which gives a quantitative measure of the two-drugs interaction, was derived as:

$$CI = \frac{C_{50,A}}{IC_{50,A}} + \frac{C_{B,50}}{IC_{50,B}} \quad (2)$$

where $C_{A,50}$ ($C_{B,50}$) is the concentration of drug A – DTXL (drug B – CURC) in combination with drug B – CURC (drug A – DTXL) at 50 % efficacy; average $IC_{50,A}$ ($IC_{50,B}$) is the concentration of DTXL alone (CURC alone) at 50 % efficacy. Note that CI > 1 represents antagonistic behavior, CI = 1 documents an additive behavior, CI < 1 implies synergistic behavior.

### 2.9. SPN intracellular uptake

For evaluating the intracellular uptake of SPN by SH-SY5Y, confocal microscopy analyses were performed. Before cell seeding, each well was pre-treated with human fibronectin and placed in incubator for 30 min at 37 °C. $8 \times 10^4$ SH-SY5Y-Luc$^+$ cells were seeded into each well of a Nunc Lab-Tek II Chamber Slide System (Thermo Fisher Scientific, USA). After 24 h, cells were incubated with a non-toxic concentration of Cy5 conjugated SPN (Cy5- SPN). After 24 h, the culturing media was removed, and cells were washed in PBS (Thermo Fisher Scientific, USA). Fixation was performed using a 3.7 % solution of PFA (Sigma-Aldrich, USA) for 5 min. Actin was stained with Alexa Fluor Phalloidin (green color) (Thermo Fisher Scientific, USA) and nuclei were stained with DAPI (blue color) (Thermo Fisher Scientific, USA) following the vendor indications. A z-stack section was acquired using a 60 × objective (≥ 12 steps of 1000 nm each were acquired per image).

Flow cytometry was performed using a FACS ARIA (Becton Dickinson, USA), as previously reported [40]. Flow cytometry was performed using a FACS ARIA (Becton Dickinson, USA), as previously reported [40]. $2 \times 10^5$ cells were seeded into each well of a 12-well plate, preserving the same conditions as per the cell culture protocol. For the 1 h internalization analyses, cells were exposed to Cy5-SPN after 47 h of culture; for the 4 h internalization analyses, cells were exposed to Cy5-SPN after 44 h of culture; and for the 24 h incubation analyses, cells were exposed to Cy5-SPN after 24 h of culture. At the end of the incubation period (48 h post-seeding for all three conditions), cells were washed using cold PBS (200 μL) and detached by gentle scraping. Samples were immediately stored in ice and vortexed right before the analysis. A cell population was selected setting a scatter gate that would exclude the negligible amounts of debris and aggregates while considering the side scatter (SSC) shifts due to the internalized particles (see Supporting information). The cell population positive for internalization was selected considering the basal level of fluorescence of the untreated cells.

### 2.10. Orthotopic murine cancer model

Female athymic Nude-Foxn1$^{nu}$ (*nu/nu*) mice (Envigo, Bresso, Italy) were housed under pathogen-free conditions. In accordance with the 3 R principles (replace, reduce, refine), experiments were reviewed and approved by the licensing and ethical committee of the Ospedale Policlinico San Martino and the Italian Ministry of Health (n. 661/2016-PR and 883/2020-PR). Luc-transfected SH-SY5Y (SH-SY5Y-Luc+) cells ($10^6$ cells in 10 μL culture medium) were inoculated in the left adrenal gland of five-week-old *nu/nu* mice, as previously described by the authors [41,42]. Mice body weight and general physical status were daily recorded. When any sign of discomfort or poor health arose (*i.e.*, abdominal

dilatation, dehydration, paraplegia, > 20 % weight loss), mice were anaesthetized with xilezine (Xilor 2 %, Bio98 Srl, Milan, Italy) and sacrificed by $CO_2$ inhalation. The day of euthanasia was recorded as the day of death.

### 2.11. In vivo therapeutic experiments

Bioluminescence imaging (BLI) and survival were used to determine the efficacy of the treatment. Seven days after SH-SY5Y-Luc$^+$ cell inoculation, mice were randomly assigned to different groups after BLI evaluation ((n = 11/group) and iv (intravenously) treated with 3 mg/kg DTXL-SPN, 1.5 mg/kg CURC-SPN, and drug combination CURC/DTXL-SPN, three times per week. The treatment lasted 3 and 4 weeks in total for BLI (4 mice/group) and survival experiments (7 mice/group), respectively. In another set of experiments, SH-SY5Y-Luc$^+$ bearing mice (4 mice/group) were treated with the free molecular form of the drugs, with the same dosing. In all the *in vivo* experiments, control mice (CTR) received saline. Mice were weighed 24 h after each treatment.

In the toxicity experiments, tumor-bearing mice (n = 3/group) were anesthetized with xylazine 24 h after the last day of SPN treatments and blood was collected, as previously reported by the authors [37]. Hematological levels of red blood cells (RBC), reticulocytes (RET), hematocrit (HCT), hemoglobin (HGB), white blood cells (WBC) and platelets (PLT), as well as clinical chemistry levels of serum albumin (ALB), phosphatase alkaline (ALP), glutamic-pyruvic transaminase (ALT), glutamic oxaloacetic transaminase (AST), lactate dehydrogenase (LDH), creatine phosphokinase (CK), creatinine (CREA) and urea were quantified. Hematological analyses were performed at the Mouse Clinic of the IRCCS Ospedale San Raffaele (Milano).

*In vivo* experiments were blindly executed at the Animal Facility of the IRCCS Ospedale Policlinico San Martino, Genoa, Italy, using nanoparticles synthesized in the Laboratory of Nanotechnology for Precision Medicine, Fondazione Istituto Italiano di Tecnologia, Genoa, Italy. Data are expressed as mean ± SD. Differential findings among the experimental conditions were determined by one-way ANOVA analysis of variance, with Tukey's multiple comparison test, using GraphPad Prism 5 (GraphPad Software v5.0, San Diego, CA, USA). Survival curves were drawn as Kaplan-Meier Cumulative Proportion Surviving graphs, and corresponding p-values were calculated by the use of the log-rank (Mantel-Cox) test. Stars indicate the following p-value ranges: ** = $p < 0.01$.

### 2.12. SPN biodistribution and PET/MR imaging experiments

One week after inoculation with SH-SY5Y-Luc$^+$ cell, 15 mice were randomly divided into two groups: control mice (n = 9 mice) and treated mice (n = 6 mice). From the control group, n = 3 mice were injected with SPN labeled with $^{64}$Cu to assess particle biodistribution before beginning of the treatments. The remaining 12 mice were either injected with saline (6 remaining control mice) or treated with CURC/DTXL-SPN (6 treated mice). Saline and particle administration was performed every two days for a total of 4 injections (100 μL of combined CURC/DTXL-SPN with 3 mg/kg DTXL and 1.5 mg/kg CURC concentration, through retro-orbital injection). MR imaging and biodistribution analyses were performed at the end of the treatment and one week after the end of the treatment.

For MR imaging, a sequential MRS-PET 7T system (MRSolutions, UK) was used. This system associates a 7T cryogen free magnet MRS with a clip-on SiPM PET ring. MRI acquisitions (scout images followed by a fast spin echo - FSE T1w: TE 11 ms; TR 1100 ms; 0.8 mm slice thickness - acquired in the axial plane) were performed sequentially. Animal respiration was monitored with an abdominal pressure sensor and dedicated software (PC Sam, SAII, Stony Brook).

For the PET biodistribution analyses, 24 h upon injection of $^{64}$Cu-SPN (100 μCi), mice were euthanized, and the organs were collected and weighed. The radioactivity was measured with a scintillation γ-counter (WIZARD 2480, PerkinElmer, Waltham, MA).

## 3. Results

### 3.1. Synthesis and in vitro characterization of the spherical polymeric nanomedicines

An oil-in-water emulsion/solvent evaporation technique, previously reported by the authors [13,35], was used to synthesize the spherical polymeric nanomedicines (SPN). These comprise a poly (lactic-co-glycolic acid) (PLGA) core within which the hydrophobic drug molecules curcumin (CURC) and docetaxel (DTXL), either alone or in combination, were encapsulated. This hydrophobic polymeric core was stabilized by a lipid surface monolayer comprising DPPC (7.5 % w/w) and DSPE-PEG (9.2 % w/w). Fig. 1**A** provides a schematic representation of the SPN. As reported *via* scanning electron microscopy (SEM) analysis, SPN show a regular spherical shape and a quite homogeneous size distribution (Fig. 1**B**). The particle size was also evaluated using a dynamic light scattering system. Both empty and drug-loaded nanoparticles presented an average hydrodynamic diameter of about 185 nm with a narrow size distribution (PdI < 0.15), as listed in the table of Fig. 1**C**. The hydrodynamic diameter of SPN was not affected by the encapsulation of the therapeutic molecules (CURC or DTXL, either alone or in combination), dispersed within the PLGA polymeric core, in accordance with what was previously reported by the authors in the case of other drug molecules [35]. Also, the surface ζ-potential for all the developed formulations was around - 40 mV, as dictated by the carboxylic groups exposed on the termini of DSPE-PEG chains (Fig. 1**A, C**). SPN were also characterized in terms of drug loading using standard liquid chromatographic techniques. The formulation CURC/DTXL–SPN was optimized to load CURC and DTXL in a mass ratio of 1:2, as the chemotherapeutic molecule has the highest cytotoxic potential. As listed in Fig. 1**C**, a CURC/DTXL–SPN formulation contained 185.98 ± 18.76 μg and 381.13 ± 78.33 μg of CURC and DTXL, respectively. On the other hand, when CURC or DTXL were loaded alone in the SPN, the amounts of CURC or DTXL were slightly higher and equal to 224.26 ± 38.01 μg and 490.62 ± 91.22 μg, respectively.

SPN colloidal stability was assessed under physiological conditions. All the formulations listed in Fig. 1**C** were resuspended in PBS (pH = 7.4, 37 °C) and their hydrodynamic size and size distribution were monitored up to 4 days. Data in Fig. 1**D** show that all the formulations were stable, preserving their average size and PDI over the entire observation period.

To complete the *in vitro* characterization of the SPN, release studies of CURC and DTXL were performed in PBS (pH = 7.4, 37 °C) up to 72 h post-incubation. The release profiles of CURC (red line) and DTXL (blue line) co-loaded into SPN are reported in Fig. 1**E**. A biphasic rapid/slow release profile was observed for both drugs, with almost 90 % of the total mass released within the first 24 h. Similar release profiles were reported for CURC–SPN and DTXL–SPN in the monotherapy formulations (Supporting Fig. S1). As previously reported by the same authors, the CURC release profile appeared to be faster that DTXL, either alone or in combination, probably due to the smaller molecular weight of the natural compound (CURC: 368.4 Da *vs* DTXL: 807.9 Da) [13,40]. A comparison among the release profiles would suggest a slower release of DTXL, when combined with CURC (Supporting Fig. S1). This could be due to the different interaction of DTXL and CURC with PLGA matrix, when are co-loaded in the same particles. However, the difference in the DTXL amount released from the combined system is smaller than 10 %.

### 3.2. Cytotoxic potential and uptake in neuroblastoma cells of the CURC/DTXL – SPN

First, the combination of the potent anti-cancer drug docetaxel (DTXL) and anti-inflammatory molecule curcumin (CURC) was tested on a panel of human cell lines. Specifically, the viability of the SH-SY5Y-

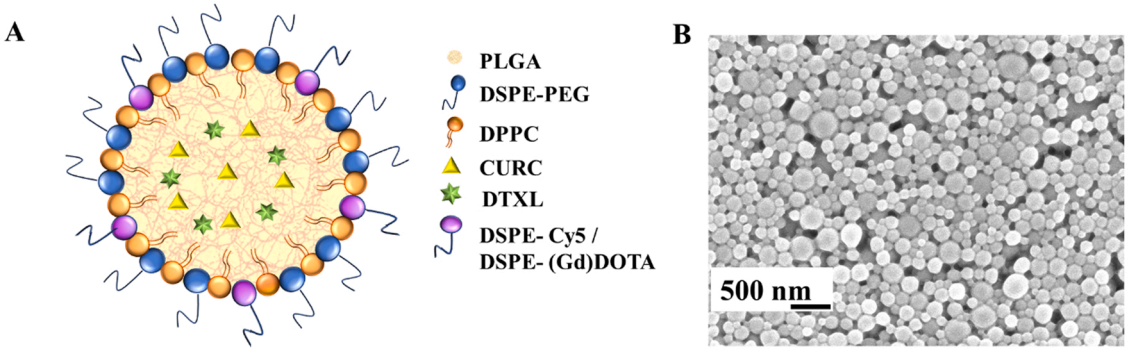


C

| Sample | Physico-chemical features | | | Drug loading (μg) | |
|---|---|---|---|---|---|
| | Size (nm) | PdI[a] | ζ-Pot (mV) | DTXL | CURC |
| Empty- SPN | 191.44 ± 9.60 | 0.07 ± 0.02 | -45.50 ± 1.86 | ----- | ----- |
| DTXL-SPN | 183.00 ± 3.20 | 0.13 ± 0.01 | -44.40 ± 3.44 | 490.62 ± 91.22 | ----- |
| CURC-SPN | 192.90 ± 5.29 | 0.06 ± 0.02 | -39.50 ± 3.53 | ----- | 224.26 ± 38.01 |
| CURC/DTXL-SPN | 183.00 ± 3.20 | 0.13 ± 0.01 | -44.00 ± 3.01 | 381.13 ± 78.33 | 185.98 ± 18.76 |

[a] Polidispersity index;

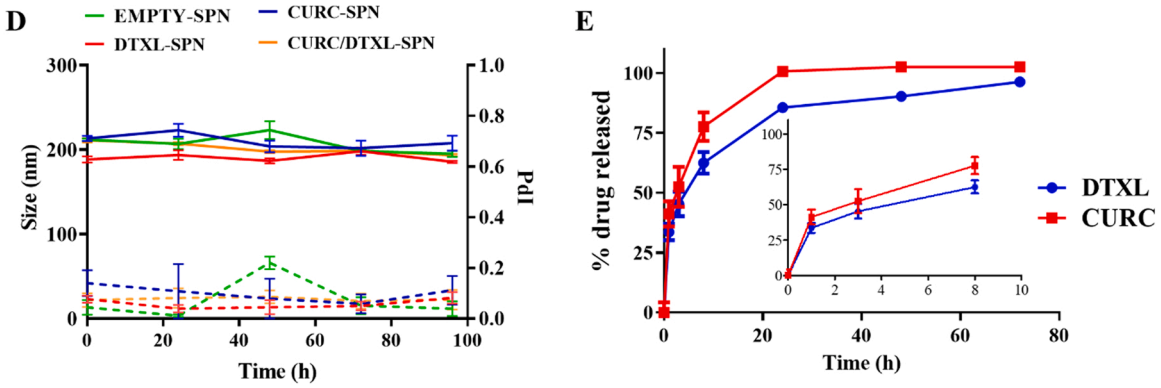


**Fig. 1. Physico-chemical and pharmaceutical characterization of the spherical polymeric nanomedicine. A.** Schematic representation of a Spherical Polymeric Nanomedicine (SPN) showing its core and surface architecture; **B.** A representative SEM image of empty SPN; **C.** Physico-chemical and drug loading characterization of SPN; **D.** SPN stability over time at 37 °C (size: solid lines; PdI: dashed lines); **E.** Release profiles for CURC and DTXL from CURC/DTXL-SPN (in PBS, pH 7.4, 37 °C). Data presented as mean ± SD (n = 3).

$Luc^+$ cells was tested against six therapeutic groups, including free CURC, free DTXL, and their combination free CURC/DTXL (1:2 ratio); the nano-formulated CURC-SPN, DTXL-SPN, and their combination CURC/DTXL-SPN (1:2 ratio). Fig. 2**A, B** display the cell viability at different concentrations and predefined time points for the free CURC/DTXL and CURC/DTXL-SPN, respectively. Similar data are presented for the other therapeutic groups in the Supporting information (the free CURC and free DTXL cases are reported in Supporting Fig. S2 A–C, respectively; the CURC-SPN and DTXL-SPN cases are presented in Supporting Fig. S2 B–D, respectively). In all the analyzed cases, it is confirmed that the cytotoxic effect is dose- and time-dependent: the higher the dose and the longer the exposure time, the larger the number of dead cells. From these cell viability charts, $IC_{50}$ values can be derived for the three different time points, as listed in the table of Fig. 2**C**.

For demonstrating the synergism between DTXL and CURC, the viability of SH-SY5Y-$Luc^+$ exposed to a non-toxic CURC concentration (namely 2 μM) and DTXL was first assessed (Supporting Fig. S4 A). Under this condition, the combination of DTXL and CURC resulted to be more effective than the corresponding monotherapies (Supporting Fig. S2 A, C). Based on this, SH-SY5Y-$Luc^+$ cytotoxicity was assessed again using CURC/DTXL-SPN and their free combination with a fixed mass ratio of CURC:DTXL 1:2, loaded in the SPN. The Combination Index (CI) values listed in Fig. 2**C** confirmed the synergism between CURC and DTXL on SH-SY5Y-$Luc^+$. The CI is equal to 0.54 for the free CURC/DTXL combination and 0.65 for the CURC/DTXL-SPN. By comparing the $IC_{50}$ values among the tested therapeutic groups, it can be concluded that the encapsulation of the two drugs, in combination or individually, into the SPN is generally associated with a higher cytotoxic effect. For instance, at 72 h, a treatment with CURC/DTXL-SPN returned a $IC_{50} = 2.10 \pm 0.10$ nM as opposed to 6.40 ± 0.90 nM for free DTXL or 3.16 ± 0.09 nM for DTXL-SPN. For free CURC, the $IC_{50}$ was equal to 2989.50 ± 0.70 nM at 72 h *vs* 1898.50 ± 215.70 nM for CURC-SPN. Moreover, the cytotoxicity of empty SPN was also assessed upon incubation with SH-SY5Y cells and returning a cell viability higher than 80 % at any of the tested SPN concentrations and time points (Supporting Fig. S3), in agreement with previous reports from the authors [43–46].

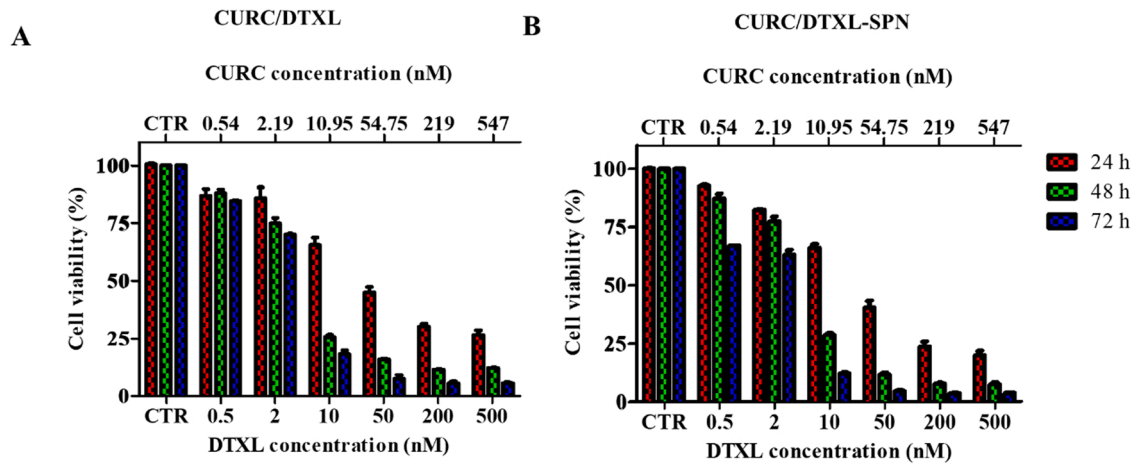


C

| | IC $_{50}$ (nM) | | | CI |
|---|---|---|---|---|
| **Sample** | **24 h** | **48 h** | **72h** | **72h** |
| **DTXL** | 43.90 ± 8.10 | 11.20 ± 2.90 | 6.40 ± 0.90 | |
| **CURC** | 6,168.00 ± 453.00 | 4,169.50 ± 600.30 | 2,989.50 ± 0.70 | |
| **DTXL-SPN** | 22.60 ± 5.00 | 3.00 ± 0.30 | 3.16 ± 0.09 | |
| **CURC- SPN** | 6,517.00 ± 1,026.70 | 2,789.00 ± 158.40 | 1,898.50 ± 215.70 | |
| **CURC/DTXL (DTXL)** | 42.50 ± 6.30 | 4.80 ± 1.10 | 3.40 ± 0.04 | 0.54 |
| **CURC/DTXL (CURC)** | 46.50 ± 6.90 | 5.20 ± 1.20 | 3.70 ± 0.02 | 0.54 |
| **CURC/DTXL- SPN (DTXL)** | 32.60 ± 13.30 | 4.90 ± 0.60 | 2.10 ± 0.10 | 0.65 |
| **CURC/DTXL- SPN (CURC)** | 35.70 ± 14.60 | 5.60 ± 1.00 | 2.30 ± 0.20 | 0.65 |

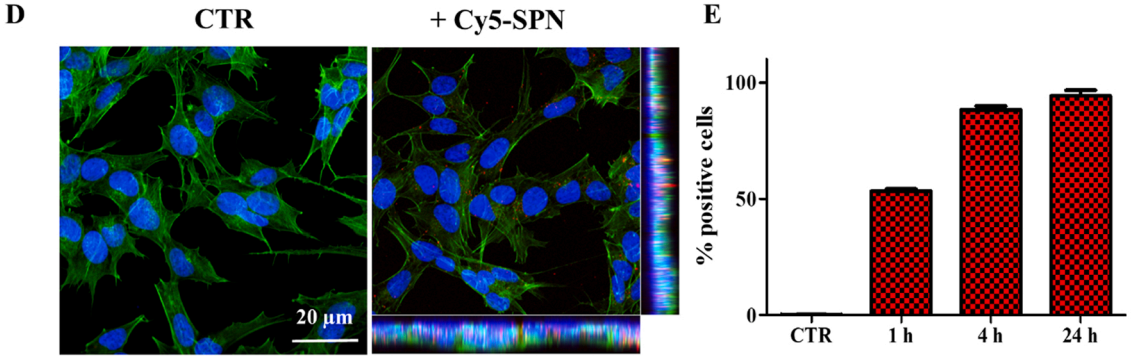


**Fig. 2. Cytotoxicity and intracellular accumulation of the Spherical Polymeric Nanomedicines. A.** and **B.** SH-SY5Y-Luc$^{+}$ cell viability upon incubation with free CURC/DTXL and CURC/DTXL-SPN. **C.** $IC_{50}$ values for the different therapeutic groups at 24, 48 and 72 h on SH-SY5Y-Luc$^{+}$ cells and corresponding CI values for the combination groups. ($IC_{50}$ values for the combination groups are referred to the drug noted in parenthesis). **D.** Representative confocal images of SH-SY5Y- Luc$^{+}$ not incubated (CTR – **left**) and incubated (Cy5-SPN - **right**) with Cy5-SPN for 24 h (scale bar: 20 µm). **E.** Flow cytometry analysis SH-SY5Y- Luc$^{+}$ exposed to Cy5-SPN for 1, 4 and 24 h. Data presented as mean ± SD (n = 3).

Similar trends in terms of cell viability after exposure to CURC and DTXL were also documented for the other three neuroblastoma cell lines, LAN-5, HTLA-230 and IMR-32, as demonstrated in the Supporting Figs. S4 B–D and S5–7. Interestingly, the CURC/DTXL synergism was confirmed on all the cell lines, except for the IMR-32 where DTXL alone already induced a strong cytotoxic effect with an $IC_{50}$ = 0.09 nM at 72 h, suggesting that these cells do not develop any significant resistance to DTXL. Incidentally, given the different origin of the four neuroblastoma cell lines, this data would continue to highlight the relevance of the proposed combination therapy possibly across different neuroblastoma patients.

Indeed, the co-encapsulation of two poorly water-soluble drugs into a single nanoparticle is expected to enhance cellular uptake and intracellular drug accumulation, thus boosting the cytotoxic effect [47–49]. Therefore, the time-dependent nanoparticle internalization into SH-SY5Y was studied *via* confocal fluorescent microscopy and flow cytometry analyses. For these experiments, SPN were labeled with the near-infrared probe Cy5 by intercalating a Cy5-conjugated phospholipid molecules (DSPE-Cy5) within the lipid monolayer (Fig. 1**A**). As reported in Fig. 2**D** and Supporting Fig. S8, cancer cells (blue cell nuclei – DAPI and green filamentous actin – Alexa Fluor 488 Phalloidin) rapidly took up nanoparticles (red dots), which tended to accumulate perinuclearly

as confirmed by the confocal Z-stack analyses [35]. This was also documented and quantified *via* flow cytometry (Fig. 2**E** and Supporting Fig. S9). The percentage of SH-SY5Y-Luc$^{+}$ associated with SPN (*i.e.*, percentage of positive events) for the three tested time points (1, 4, and 24 h) was 53.33 ± 0.88, 88.30 ± 1.55, and 94.15 ± 2.48%, respectively.

### 3.3. Therapeutic efficacy in orthotopic models of neuroblastoma

The antitumor efficacy of the proposed drug combination was evaluated in an orthotopic model of neuroblastoma. $10^6$ Luc-transfected SH-SY5Y (SH-SY5Y-Luc$^{+}$) cells were inoculated in the left adrenal gland of five-week-old *nu/nu* mice. Notably, this model accurately recapitulates tumor growth and metastatic spreading clinically observed in relapsed/refractory neuroblastoma patients [39,41,42]. Tumor growth and response to the treatment were monitored *via* Bioluminescent Imaging (BLI) and survival, following the schematic of Fig. 3**A.**

Representative BLI images for control mice (CTR) and the nano-formulated therapeutic groups are provided in Fig. 3**B** at 24 h post the 9th treatment (after 3 weeks of treatment). Photon counts in the tumor region of interest (ROI) show that DTXL-SPN, CURC-SPN and CURC/DTXL-SPN significantly delay tumor growth compared to CTR mice and empty-SPN ($p = 0.0071$) (Fig. 3**C**). Kaplan-Meyer survival curves associated with a 4-week long treatment (12 administrations) were evaluated for all different therapeutic groups (Fig. 3**D**). As expected, no statistical significant difference was detected when comparing the CTR and empty-SPN-treated mice. However, compared to CTR mice, both DTXL-SPN and CURC-SPN treatments delayed tumor growth (DTXL-SPN *vs* CTR: $p = 0.0062$; CURC-SPN *vs* CTR: $p = 0.0474$). As anticipated from the *in vitro* cellular assays, the efficacy of the combination CURC/DTXL-SPN was confirmed to be stronger compared to the nano-formulated monotherapies (CURC/DTXL-SPN *vs* CURC-SPN: $p = 0.00205$; CURC/DTXL-SPN *vs* DTXL-SPN: $p = 0.00391$) and CTR (CURC/DTXL-SPN vs CTR: $p = 0.0002$) (see tables in Fig. 3**D**). Of note, treatments performed with the free drugs did not exert any therapeutic effect (free DTXL *vs* CTR: $p = 0.3011$; free CURC *vs* CTR: $p = 0.4250$; free CURC/DTXL *vs* CTR: $p = 0.7655$, Supporting Fig. S10), most likely for the poor bioavailability of DTXL and CURC (Supporting Fig. S11**)**. No weight loss (data not shown) or chronic hematological (Supporting Fig. S12**)** and clinical chemistry (Fig. 3**E** and Supporting Fig. S13) toxicities emerged by the quantification of the corresponding markers in blood and plasma, respectively.

### 3.4. Magnetic Resonance imaging and biodistribution

Tumor imaging and SPN biodistribution were evaluated for the orthotopic NB model described above. Tumors were left to grow for one week before splitting the mice into two groups: control, untreated mice (n = 9) and treated mice (n = 6). The treated mice received an intravenous injection of CURC/DTXL-SPN every 2 days, starting on day 7 from NB cell inoculation, up to a total of 4 injections. Following the timeline of Fig. 4**A** and Supporting Fig. 14, MR images were taken on day 7, 14, and 21 post tumor cell inoculation and the development of the tumor mass was monitored over time. In the control, untreated mice (CTR), the tumor size increased from 6 ± 5.2 $mm^3$ at day 7–75 ± 30 $mm^3$ at day 14, and 233 ± 71 $mm^3$ at day 21. For the treated mice, the tumor volume was 40 ± 2 $mm^3$ at day 14 and 60 ± 10.1 $mm^3$ at day 21. This MRI data (Fig. 4**B – right**) correlates with the actual mass of the tumor measured *ex-vivo* post animal sacrifice (Fig. 4**B – left**). It is evident the dramatic reduction in tumor mass following a 1-week treatment with the CURC/DTXL-SPN. Indeed, interrupting the treatment at 1-week resulted in tumor progression, although the malignant mass stayed smaller than the untreated control for the whole observation period.

Following each MR imaging session, 100 μCi of $^{64}$Cu-labeled SPN ($^{64}$Cu-SPN) were injected systemically to assess nanoparticle accumulation in the relevant organs, including the organs of the reticulo-endothelial system (RES) (liver, spleen, kidneys, and lungs), the brain, the right kidney with no tumor, the left kidney with tumor, and the tumor itself. At 24 h post nanoparticle injection, mice were euthanized, and the relevant organs were collected and weighted. As already documented in previous works by the authors and others, a significant dose of the injected nanoparticles was detected in the RES organs [50]. At 8 days post tumor cell inoculation, the percentage of injected SPN normalized by the mass of the organ (% ID/g) was equal to 45 ± 7.1 % ID/g in the liver, 26 ± 7 % ID/g in the spleen, and 4.9 ± 0.6 % ID/g in the kidneys. Over time minor and not significant changes were observed in $^{64}$Cu-SPN accumulation within these organs, for both untreated and treated mice (Fig. 4**C**). For the tumor, a SPN accumulation of 2.3 ± 0.5 % ID/g was measured at day 8 post cell inoculation. The SPN accumulation did not change significantly over time and, at day 15 and 22 post cell inoculation, was equal to 1.6 ± 0.3 and 2.02 ± 0.22 % ID/g for the untreated mice, and 1.8 ± 0.23 and 1.7 ± 0.6 % ID/g for the 1-week treated mice. Importantly, the observed time-independent and quasi-constant intratumor deposition of SPN is fundamental to ensure a continuous supply of therapeutic molecules and treatment efficacy.

## 4. Discussion

Spherical polymeric nanomedicines (SPN) presenting a solid core made of a hydrophobic polymer, like PLGA, externally stabilized by a lipid layer have been proposed by the authors and others for the delivery of water insoluble small molecules, inhibitors, and therapeutic drugs for a variety of medical conditions [40,51]. Indeed, similar particles can also be realized with other more exotic polymers [43]. However, the authors have chosen PLGA because it is one of the most versatile FDA-approved biodegradable polymers, which has been already extensively used for the delivery of various small molecules, proteins and macromolecules [52,53]. Its biocompatibility and moderate toxicity are key factors. When expose to biological fluids, PLGA progressively hydrolyzes becoming lactic acid and glycolic that enter the cycle of Kreb to be eventually eliminated as $CO_2$ and water. Furthermore, the overall physical properties of the polymer-drug matrix can be tuned by acting directly on the PLGA specific features, such as the polymer molecular weight and the lactic-to-glycolic acid ratio. In this specific work, a 50:50 PLA/PGA mixtures was selected as this is the most extensively used configuration in medical applications for its fast degradation kinetics [53].

It should also be mentioned that, often, given their characteristic spherical shape and size of 200 nm, SPN have been used as a benchmark for the development of novel drug delivery systems [14,54,55]. In the current work, SPN are used for the systemic administration of two water insoluble molecular agents – CURC and DTXL – in the treatment of a highly aggressive and currently uncurable pediatric tumor – neuroblastoma. Orthotopic neuroblastoma models are complex preclinical models that requires an invasive and delicate surgical procedure to precisely inoculate the cancer cells of choice in the adrenal gland of a mouse.

In a previous work by the authors [13], SPN were co-loaded with CURC and DTXL and used for the treatment of a non-orthotopic brain tumor. At first sight, the two nanocarriers may appear similar but, in Stigliano and colleagues [13], SPN were synthetized through a nano-precipitation process while, in the current work, an oil-in-water emulsion/solvent evaporation technique is adopted. The revised fabrication approach provides several significant advantages. First, it allowed the authors to work always at room temperature avoiding the synthesis of particles in pre-heated solutions up to 65 °C. Second, the emulsion/evaporation technique enabled the use of highly volatile solvents, like chloroform as opposed to ethanol and acetonitrile, thus facilitating the purification process and ensuring that no residual traces of toxic solvents are left in the final preparation. Third, it gave the authors the opportunity to modify the ratio between the two molecular agents leading to the realization of SPN enriched in the chemotherapeutic drug DTXL over

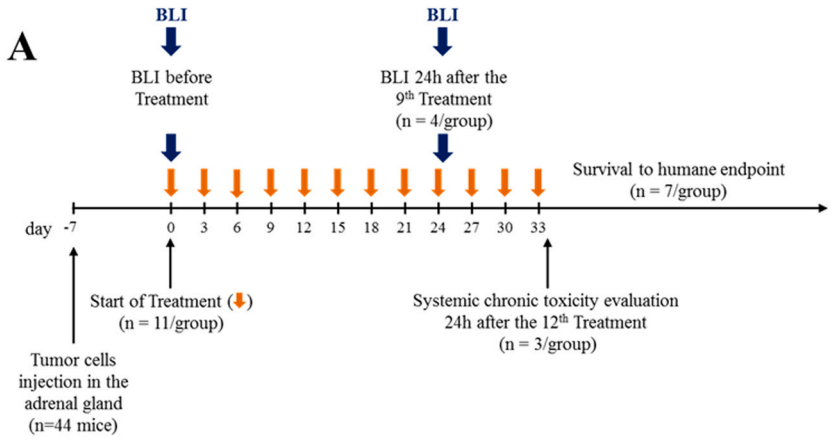


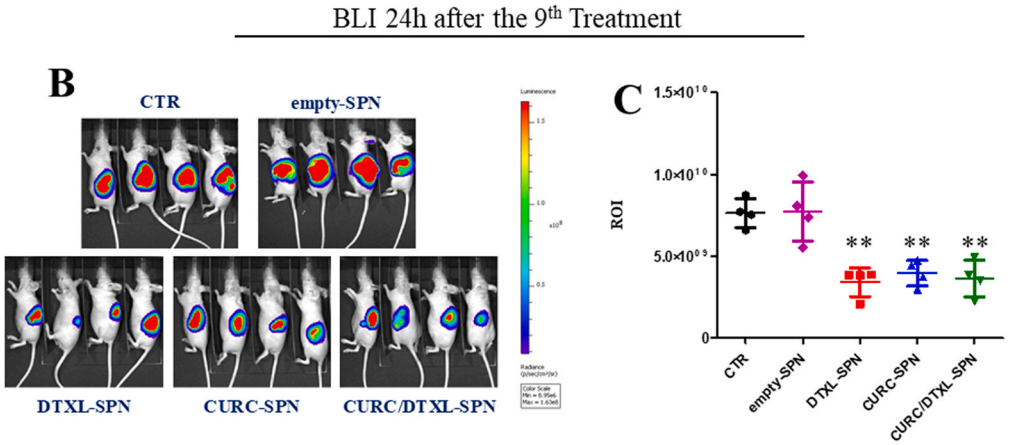


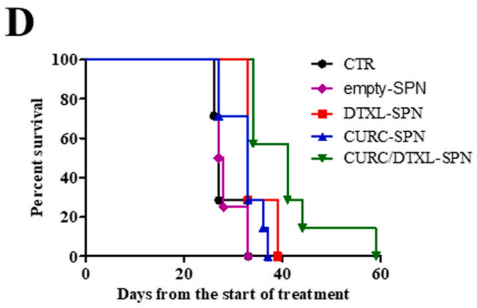


| Groups | Median Survival (days) | Statistic (*vs* CTR) | Statistic (CURC/DTXL-SPN *vs* SPN monotherapy) |
|---|---|---|---|
| CTR | 27 | | |
| empty-SPN | 27.5 | n.s. | |
| DTXL-SPN | 33 | $p = 0.0062$ | $p = 0.00391$ |
| CURC-SPN | 33 | $p = 0.0474$ | $p = 0.00205$ |
| CURC/DTXL-SPN | 41 | $p = 0.0002$ | |

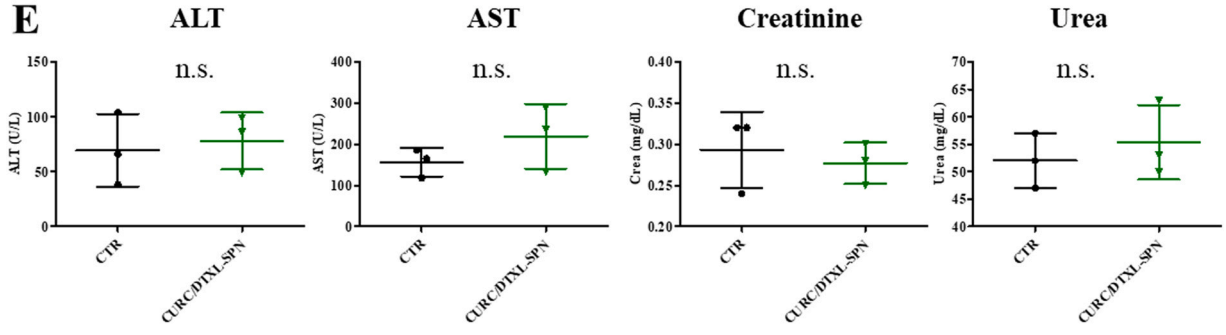


**Fig. 3. Therapeutic efficacy in orthotopic models of neuroblastoma. A.** Schematic and timeline of the *in vivo* experiments. $10^6$ cells/10 μL medium were orthotopically inoculated in the left adrenal gland of mice (n = 11/group). Treatment started 7 days post cell inoculation and were performed 3 times/week for a total of 12 administrations. **B.** Representative bioluminescence imaging (BLI) taken 3 weeks post treatment initiation (24 h post 9th administration) for the 3 nano-formulated therapeutic groups (CURC-SPN; DTXL-SPN; and CURC/DTXL-SPN), the empty nanoparticles (empty-SPN), and the untreated control (CTR). **C.** Corresponding photon counts within the tumor region of interest (**: $p < 0.01$, DTXL-SPN, CURC-SPN; CURC/DTXL-SPN *vs* CTR and *vs* empty-SPN). **D.** Kaplan-Meyer survival curves with corresponding statistical analysis comparing the nano-formulated therapeutic groups against CTR and empty-SPN. **E.** Levels of glutamic-pyruvic transaminase (ALT), glutamic oxaloacetic transaminase (AST), creatinine (CREA) and UREA at 24 h post last 4-weeks treatment. (Statistics: CURC/DTXL-SPN *vs* CTR, not significant (n.s.)). Data presented as mean (n = 3) ± SD.

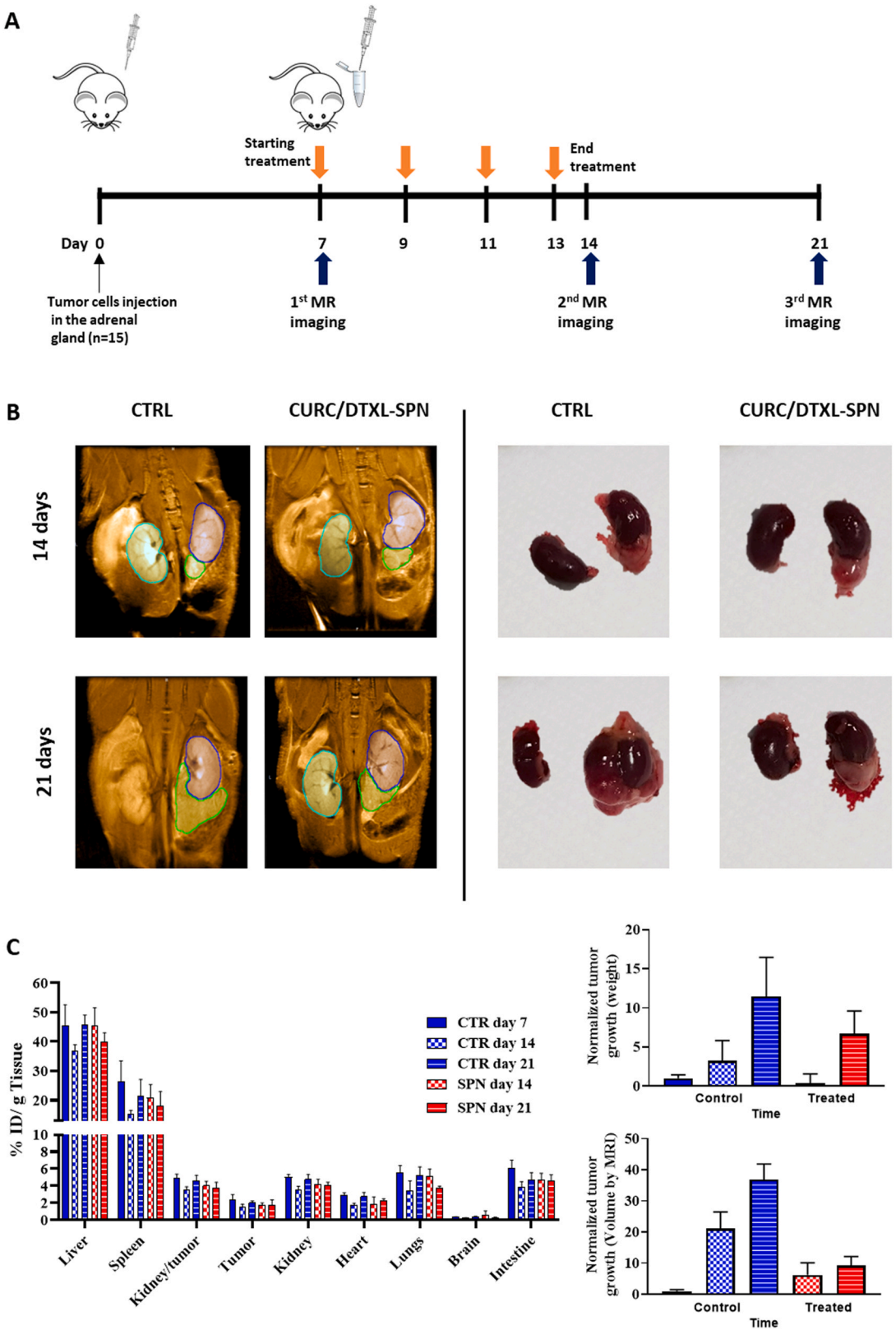


**Fig. 4. Magnetic resonance imaging of the tumor and SPN biodistribution analyses. A.** Timeline for the imaging analyses, performed on 1-week long CURC/DTXL-SPN treated or untreated (CTR) mice ($n \geq 6$). **B.** Tumor burden assessed longitudinally in time *via* MR imaging (**left**) and *ex-vivo* weight measurements (**right**) (green area: tumor; light blue area: left kidney with tumor; dark blue area: right kidney with no tumor). **C.** Biodistribution analysis of $^{64}$Cu-SPNs at 0, 1 and 2 weeks (**left**). Tumor mass growth, normalized by CTR at time 0, as measured *ex-vivo* by mass (weight) (**right, top**) and longitudinally *via* MR imaging (**right, bottom**).

the broad anti-inflammatory molecule CURC. Indeed, in the current configuration SPN have a CURC:DTXL mass ratio of 1:2, in contrast with the previous work of Stigliano and collaborators where CURC and DTXL were encapsulated in equal parts (CURC:DTXL mass ratio 1:1). All this resulted in different physico-chemical properties of the particles too, with the current SPN being slight larger in hydrodynamic diameter.

It is here also important to highlight that the synergistic effect of the CURC/DTXL combination tends to manifest on different cancer cells. This might be due to several reasons including the fact that CURC is known to down-regulate the expression of the transcription factor NF-κB, which is overexpressed in a variety of cancer cells and is often associated with resistance to chemotherapy, as previously documented by the authors in the case of the glioblastoma cell line U87-MG [13]. In addition to this work, more recently other authors have reported the potency of a similar combination. For instance, Banerjee et al. evaluated the effect of CURC and DTXL on different pancreatic cancer cell lines, including DU145 and PC3, showing that the combined treatment inhibited proliferation and induced significantly higher apoptosis [56]. They also commented on the fact that the combination modulated the expression of several molecules, including NF-κB, p53, and COX-2. Also, Hu and colleagues co-delivered DTXL and CURC using nanomicelles for the treatment of ovarian cancer [57]. The ~ 40 nm micelles exhibited a stronger cytotoxic effect on A2780 cells as well as *in vivo* as compared to DTLX or CURC alone. The authors proposed that the observed synergism could be due to the CURC inhibition of the cytochrome CYP3A enzyme, which metabolizes DTXL; or the P-glycoprotein (P-gp)-a, which is associated with drug resistance. Even in this work, the activation of NF-κB and its correlation with drug resistance was noted. Finally, the very recent work of Kim et al. who co-loaded CURC and DTXL in nanostructured lipid carriers for the treatment of breast cancer [58]. A strong synergism was documented for a DTXL/CURC ratio of 1:3 (w/w) on the MCF7 and OVCAR3 cell lines and related murine mouse models.

## 5. Conclusions

The potent anti-cancer drug docetaxel (DTXL) and the broad-spectrum anti-inflammatory molecule curcumin (CURC) were co-encapsulated into biodegradable, spherical polymeric nanomedicines (SPN) for the treatment of neuroblastoma. The overall size and polydispersity index of SPN was not significantly affected by the co-loading of the two therapeutic molecules, in the mass ratio 1:2 (DTXL:CURC), due to the strongly hydrophobic matrix (PLGA) constituting the SPN core. Similarly, the release profile of the two molecules was not affected by the co-loading with most of the drug amount being released within the first 24 h post incubation.

Cytotoxic experiments conducted by exposing three free-drug groups (DTXL, CURC, and CURC/DTXL) and the corresponding nano-formulated groups to four different neuroblastoma cell lines showed the strong synergism between DTXL and CURC, with combination indexes (CI) in the range of 0.5, and the advantage of using nano-formulated as opposed to free molecules. In general, $IC_{50}$ values in the range of 1 nM were measured at 72 h post incubation.

The higher potency of the nano-formulated therapy over conventional chemotherapy was demonstrated in an accurate preclinical model of the human disease using both bioluminescence imaging, magnetic resonance imaging, and survival. Specifically, the combination CURC/DTXL-SPN returned a 41-day survival as opposed to a 27-day survival registered for the untreated and free drug treated groups. Importantly, this therapeutic effect was associated with a significant, but still sub-optimal, 2 % ID/g intratumor accumulation of the systemically administered SPN, as demonstrated *via* nuclear imaging at different stages of tumor development. No systemic toxicity was associated with the delivered therapeutic approach. In conclusion, these results show that the nano-formulation of curcumin and docetaxel holds great potential in the effective treatment of neuroblastoma. Future studies should aim at increasing the SPN tumor accumulation, by using specific targeting moieties, and loading, by developing ad hoc drug conjugates, as this will enhance the intratumor deposition of the two therapeutic molecules.

## CRediT authorship contribution statement

All the authors contributed to the study conception and design and data analysis. MDF, MF, AF synthesized and characterized SPN; CC, LDM commented on the SPN synthesis and characterization; MDF, AF conducted cell viability experiments; VDF performed internalization studies; MF, ALP conducted MR and PET imaging studies; FP, MC, VB performed all the in vivo therapeutic experiments; MDF, MF, FP, MP, PD wrote the manuscript; MP, PD oversaw all the activities. All the authors read and commented on the manuscript.

## Declaration of Competing Interest

The authors declare that they have no known competing financial interests or personal relationships that could have appeared to influence the work reported in this paper.

## Data Availability

Data will be made available on request.

## Acknowledgments

This work was partially sponsored by the project “Ligurian Alliance for Nanomedicine against cancer (PI: Paolo Decuzzi)” of the Fondazione San Paolo ; the Investigator Grant IG 2020 – ID. 24397 (PI: Fabio Pastorino) of the Associazione Italiana per la Ricerca sul Cancro (AIRC); and the Ricerca Corrente (PI: Mirco Ponzoni) by the Italian Ministry of Health. The authors acknowledge the support provided by the staff of the Material Characterization Facility at the Italian Institute of Technology.

## Appendix A. Supporting information

Supplementary data associated with this article can be found in the online version at doi:10.1016/j.phrs.2022.106639.

## References

[1] J.M. Maris, Recent advances in neuroblastoma, N. Engl. J. Med. 362 (23) (2010) 2202–2211.
[2] A. Zafar, et al., Molecular targeting therapies for neuroblastoma: progress and challenges, Med. Res. Rev. 41 (2) (2021) 961–1021.
[3] K.K. Matthay, et al., Neuroblastoma, Nat. Rev. Dis. Prim. 2 (1) (2016) 16078.
[4] A.C. Mertens, et al., Late mortality experience in five-year survivors of childhood and adolescent cancer: the Childhood Cancer Survivor Study, J. Clin. Oncol. 19 (13) (2001) 3163–3172.
[5] K. Bukowski, M. Kciuk, R. Kontek, Mechanisms of multidrug resistance in cancer chemotherapy, Int. J. Mol. Sci. 21 (9) (2020) 3233.
[6] K. Matthay, et al., Neuroblastoma, Nat. Rev. Dis. Prim. 2 (2016) 16078.
[7] S. Joshi, Targeting the tumor microenvironment in neuroblastoma: recent advances and future directions, Cancers 12 (8) (2020) 2057.
[8] S. Sormendi, B. Wielockx, Hypoxia pathway proteins as central mediators of metabolism in the tumor cells and their microenvironment, Front. Immunol. 9 (2018) 40.
[9] D. Hanahan, R.A. Weinberg, Hallmarks of cancer: the next generation, Cell 144 (5) (2011) 646–674.
[10] J. Boshuizen, D.S. Peeper, Rational cancer treatment combinations: an urgent clinical need, Mol. Cell 78 (6) (2020) 1002–1018.
[11] P. Fonseka, et al., Combinatorial treatment of curcumin or silibinin with doxorubicin sensitises high-risk neuroblastoma, J. Cancer Metastasis Treat. 6 (2020) 7.
[12] F. Ponthan, et al., Celecoxib prevents neuroblastoma tumor development and potentiates the effect of chemotherapeutic drugs *in vitro* and *in vivo*, Clin. Cancer Res. 13 (3) (2007) 1036–1044.
[13] C. Stigliano, et al., Radiolabeled polymeric nanoconstructs loaded with docetaxel and curcumin for cancer combinatorial therapy and nuclear imaging, Adv. Funct. Mater. 25 (22) (2015) 3371–3379.
[14] A. Lee, et al., Spherical polymeric nanoconstructs for combined chemotherapeutic and anti-inflammatory therapies, Nanomedicine 12 (7) (2016) 2139–2147.

[15] J.I. Johnsen, et al., Cyclooxygenase-2 is expressed in neuroblastoma, and nonsteroidal anti-inflammatory drugs induce apoptosis and inhibit tumor growth *in vivo*, Cancer Res. 64 (20) (2004) 7210–7215.
[16] Y. Zhi, et al., Involvement of the nuclear factor-κB signaling pathway in the regulation of CXC chemokine receptor-4 expression in neuroblastoma cells induced by tumor necrosis factor-α, Int. J. Mol. Med. 35 (2) (2015) 349–357.
[17] E. Bell, F. Ponthan, C. Whitworth, D.A. Tweddle, J. Lunec, C.P. Redfern, COX2 expression in neuroblastoma increases tumorigenicity but does not affect cell death in response to the COX2 inhibitor celecoxib, Clin. Exp. Metastasis 31 (6) (2014) 651–659.
[18] Y. Zhi, et al., NF-κB signaling pathway confers neuroblastoma cells migration and invasion ability *via* the regulation of CXCR4, Med. Sci. Monit.: Int. Med. J. Exp. Clin. Res. 20 (2014) 2746.
[19] A. Liontas, H. Yeger, Curcumin and resveratrol induce apoptosis and nuclear translocation and activation of p53 in human neuroblastoma, Anticancer Res. 24 (2B) (2004) 987–998.
[20] C. Freudlsperger, J. Greten, U. Schumacher, Curcumin induces apoptosis in human neuroblastoma cells *via* inhibition of NFκB, Anticancer Res. 28 (1A) (2008) 209–214.
[21] X. Zhang, et al., Curcumin activates Wnt/β-catenin signaling pathway through inhibiting the activity of GSK-3β in APPswe transfected SY5Y cells, Eur. J. Pharm. Sci. 42 (5) (2011) 540–546.
[22] P. Picone, et al., Curcumin induces apoptosis in human neuroblastoma cells *via* inhibition of AKT and Foxo3a nuclear translocation, Free Radic. Res. 48 (12) (2014) 1397–1408.
[23] B. Liu, L. Qu, S. Yan, Cyclooxygenase-2 promotes tumor growth and suppresses tumor immunity, Cancer Cell Int. 15 (1) (2015) 1–6.
[24] N. Hashemi Goradel, et al., Cyclooxygenase-2 in cancer: a review, J. Cell. Physiol. 234 (5) (2019) 5683–5699.
[25] H. Yin, et al., Synergistic antitumor efficiency of docetaxel and curcumin against lung cancer, Acta Biochim. Biophys. Sin. 44 (2) (2012) 147–153.
[26] T. Zwerdling, et al., Phase II investigation of docetaxel in pediatric patients with recurrent solid tumors: a report from the Children's Oncology Group, Cancer: Interdiscip. Int. J. Am. Cancer Soc. 106 (8) (2006) 1821–1828.
[27] S.M. Blaney, et al., Phase I trial of docetaxel administered as a 1-hinfusion in children with refractory solid tumors: a collaborative pediatric branch, National Cancer Institute and Children's Cancer Group trial, J. Clin. Oncol. 15 (4) (1997) 1538–1543.
[28] M.-H. Teiten, et al., Curcumin–the paradigm of a multi-target natural compound with applications in cancer prevention and treatment, Toxins 2 (1) (2010) 128–162.
[29] C. Kuo, et al., Docetaxel, bevacizumab, and gemcitabine for very high risk sarcomas in adolescents and young adults: a single-center experience, Pediatr. Blood Cancer 64 (4) (2017), e26265.
[30] J. Baker, et al., Docetaxel-related side effects and their management, Eur. J. Oncol. Nurs. 13 (1) (2009) 49–59.
[31] W. Chen, et al., Blockage of NF-kappaB by IKKbeta- or RelA-siRNA rather than the NF-kappaB super-suppressor IkappaBalpha mutant potentiates adriamycin-induced cytotoxicity in lung cancer cells, J. Cell Biochem. 105 (2) (2008) 554–561.
[32] P. Anand, et al., Curcumin and cancer: an "old-age" disease with an "age-old" solution, Cancer Lett. 267 (1) (2008) 133–164.
[33] G. Wei, et al., Recent progress in nanomedicine for enhanced cancer chemotherapy, Theranostics 11 (13) (2021) 6370.
[34] C. Rodríguez-Nogales, et al., Therapeutic opportunities in neuroblastoma using nanotechnology, J. Pharm. Exp. Ther. 370 (3) (2019) 625–635.
[35] A. Lee, et al., Spherical polymeric nanoconstructs for combined chemotherapeutic and anti-inflammatory therapies, Nanomed.: Nanotechnol. Biol. Med. 12 (7) (2016) 2139–2147.
[36] M. Di Francesco, et al., Hierarchical microplates as drug depots with controlled geometry, rigidity, and therapeutic efficacy, ACS Appl. Mater. Interfaces 10 (11) (2018) 9280–9289.
[37] C. Brignole, et al., Cell surface nucleolin represents a novel cellular target for neuroblastoma therapy, J. Exp. Clin. Cancer Res. 40 (1) (2021) 1–13.
[38] D. Di Paolo, et al., Combined replenishment of miR-34a and let-7b by targeted nanoparticles inhibits tumor growth in neuroblastoma preclinical models, Small 16 (20) (2020), 1906426.
[39] F. Pastorino, et al., Enhanced antitumor efficacy of clinical-grade vasculature-targeted liposomal doxorubicin, Clin. Cancer Res. 14 (22) (2008) 7320–7329.
[40] V. Di Francesco, et al., Modulating lipoprotein transcellular transport and atherosclerotic plaque formation in ApoE$^{-/-}$ mice *via* nanoformulated lipid–methotrexate conjugates, ACS Appl. Mater. Interfaces 12 (34) (2020) 37943–37956.
[41] F. Pastorino, et al., Vascular damage and anti-angiogenic effects of tumor vessel-targeted liposomal chemotherapy, Cancer Res. 63 (21) (2003) 7400–7409.
[42] I. Cossu, et al., Neuroblastoma-targeted nanocarriers improve drug delivery and penetration, delay tumor growth and abrogate metastatic diffusion, Biomaterials 68 (2015) 89–99.
[43] D. Di Mascolo, , et al.P. Basnett, A.L. Palange, M. Francardi, I. Roy, P. Decuzzi, Tuning core hydrophobicity of spherical polymeric nanoconstructs for docetaxel delivery, Polym. Int. 65 (7) (2016) 741–746.
[44] A. Ameruoso, R. Palomba, A.L. Palange, A. Cervadoro, A. Lee, D. Di Mascolo, P. Decuzzi, Ameliorating amyloid-β fibrils triggered inflammation *via* curcumin-loaded polymeric nanoconstructs, Front. Immunol. 8 (2017) 1411.
[45] G. Di Pompo, M. Cortini, R. Palomba, V. Di Francesco, E. Bellotti, P. Decuzzi, N. Baldini, S. Avnet, Curcumin-loaded nanoparticles impair the pro-tumor activity of acid-stressed MSC in an *in vitro* model of osteosarcoma, Int. J. Mol. Sci. 22 (11) (2021) 5760.
[46] A. Lee, D. Di Mascolo, M. Francardi, F. Piccardi, T. Bandiera, P. Decuzzi, Spherical polymeric nanoconstructs for combined chemotherapeutic and anti-inflammatory therapies, Nanomed.: Nanotechnol. Biol. Med. 12 (7) (2016) 2139–2147.
[47] J.K. Patra, et al., Nano based drug delivery systems: recent developments and future prospects, J. Nanobiotechnol. 16 (1) (2018) 1–33.
[48] R. van der Meel, et al., Smart cancer nanomedicine, Nat. Nanotechnol. 14 (11) (2019) 1007–1017.
[49] A.L. Palange, et al., Lipid–polymer nanoparticles encapsulating curcumin for modulating the vascular deposition of breast cancer cells, Nanomed.: Nanotechnol. Biol. Med. 10 (5) (2014) e991–e1002.
[50] S. Aryal, et al., Positron emitting magnetic nanoconstructs for PET/MR imaging, Small 10 (13) (2014) 2688–2696.
[51] A. Lee, et al., Dexamethasone-loaded polymeric nanoconstructs for monitoring and treating inflammatory bowel disease, Theranostics 7 (15) (2017) 3653–3666.
[52] H.K. Makadia, S.J.J.P. Siegel, Poly lactic-co-glycolic acid (PLGA) as biodegradable controlled drug delivery carrier, Polymers 3 (3) (2011) 1377–1397.
[53] E.M. Elmowafy, M. Tiboni, M.E. Soliman, Biocompatibility, biodegradation and biomedical applications of poly (lactic acid)/poly (lactic-co-glycolic acid) micro and nanoparticles, J. Pharm. Invest. 49 (4) (2019) 347–380.
[54] M. Colasuonno, et al., Erythrocyte-inspired discoidal polymeric nanoconstructs carrying tissue plasminogen activator for the enhanced lysis of blood clots, ACS Nano 12 (12) (2018) 12224–12237.
[55] M. Di Francesco, et al., Engineering shape-defined PLGA microPlates for the sustained release of anti-inflammatory molecules, J. Control Release 319 (2020) 201–212.
[56] S. Banerjee, et al., Combinatorial effect of curcumin with docetaxel modulates apoptotic and cell survival molecules in prostate cancer, Front. Biosci. (Elite Ed.) 9 (2) (2017) 235–245.
[57] Y. Hu, et al., Co-delivery of docetaxel and curcumin *via* nanomicelles for enhancing anti-ovarian cancer treatment, Int J. Nanomed. 15 (2020) 9703–9715.
[58] C.H. Kim, et al., Synergistic co-administration of docetaxel and curcumin to chemoresistant cancer cells using PEGylated and RIPL peptide-conjugated nanostructured lipid carriers, Cancer Nanotechnol. 13 (1) (2022) 17.